DIFFUSEGUIDE: GUIDING DIFFUSION MODELS MADE EASY

Anonymous authors
Paper under double-blind review

ABSTRACT

Despite advancements in conditional generation using diffusion models, conditional generation remains affected by training cost, generalizability, and speed. Training free conditional generation assists in these avenues where a model can be steered to adhere any particular condition through inference time optimization. However, existing techniques often rely on computationally intensive backpropagation through the diffusion network to estimate the guidance direction, compounded by the need for meticulous parameter tuning tailored to individual tasks. Although some recent works have introduced minimal-compute methods for linear inverse problems, a generic, lightweight guidance solution for both linear and non-linear guidance problems is still missing. To this end, we propose *DiffuseGuide*, a method that enables inference-time guidance without compute-heavy backpropagation through the diffusion network. The key idea is to approximate the guidance direction with respect to the current sample, thereby removing the backpropagation operation. Moreover, we propose an empirical guidance scale that works for a wide variety of tasks, thus removing the need for handcrafted parameter tuning. We further introduce an effective, lightweight augmentation strategy that significantly boosts performance during inference-time guidance. We present experiments using DiffuseGuide on multiple linear and non-linear tasks across multiple datasets and models to show the effectiveness of the proposed modules.

1 INTRODUCTION

Generative modeling with Denoising Diffusion Probabilistic Models (DDPMs) Sohl-Dickstein et al. (2015); Ho et al. (2020); Dhariwal & Nichol (2021); Song et al. (2021b) has improved massively over the past few years. Multiple works have extended diffusion models to text-to-image synthesis Balaji et al. (2022); Rombach et al. (2021); Saharia et al. (2022b), 3D synthesis Poole et al. (2022); Jun & Nichol (2023), video generation Ho et al. (2022); Blattmann et al. (2023); Wu et al. (2023a), as well as conditioning to solve inverse problems. Moreover, like conditional generative adversarial networks (GANs) Goodfellow et al. (2020); Arjovsky et al. (2017), DDPMs can be adapted to tasks based on a label Rombach et al. (2021); Dhariwal & Nichol (2021) or visual prior–based conditioning Saharia et al. (2022a). However, like conditional GANs Wang et al. (2018); Radford et al. (2015), DDPMs also need to be trained with annotated pairs of labels and instructions for satisfactory results. This poses a limitation in many cases where there is a lack of paired data to train large diffusion models. For this reason, there has been recent interest in models that can perform conditional generation without the need for explicit training Yu et al. (2023); Chan et al. (2016); Nguyen et al. (2017); Graikos et al. (2022).

Progressing in this direction is prior research in plug-and-play models. First introduced in Nguyen et al. (2017), the initial research on plug-and-play models Nguyen et al. (2017); Graikos et al. (2022) enabled conditional sampling from GANs trained with unlabeled data. For this, a pretrained classifier Simonyan & Zisserman (2014); Hossain et al. (2019) or a captioning model was used to estimate the deviation between the GAN-generated image and a given label; based on this deviation, the GAN input noise was modulated until the generated sample satisfied the given text or class label. A similar approach has been attempted for diffusion models to facilitate conditional sampling from unconditional diffusion models: classifier guidance Dhariwal & Nichol (2021); Graikos et al. (2022), where a noise-robust classifier is trained along with the diffusion model to guide sampling toward a particular direction. However, classifier guidance brings in the computational costs of

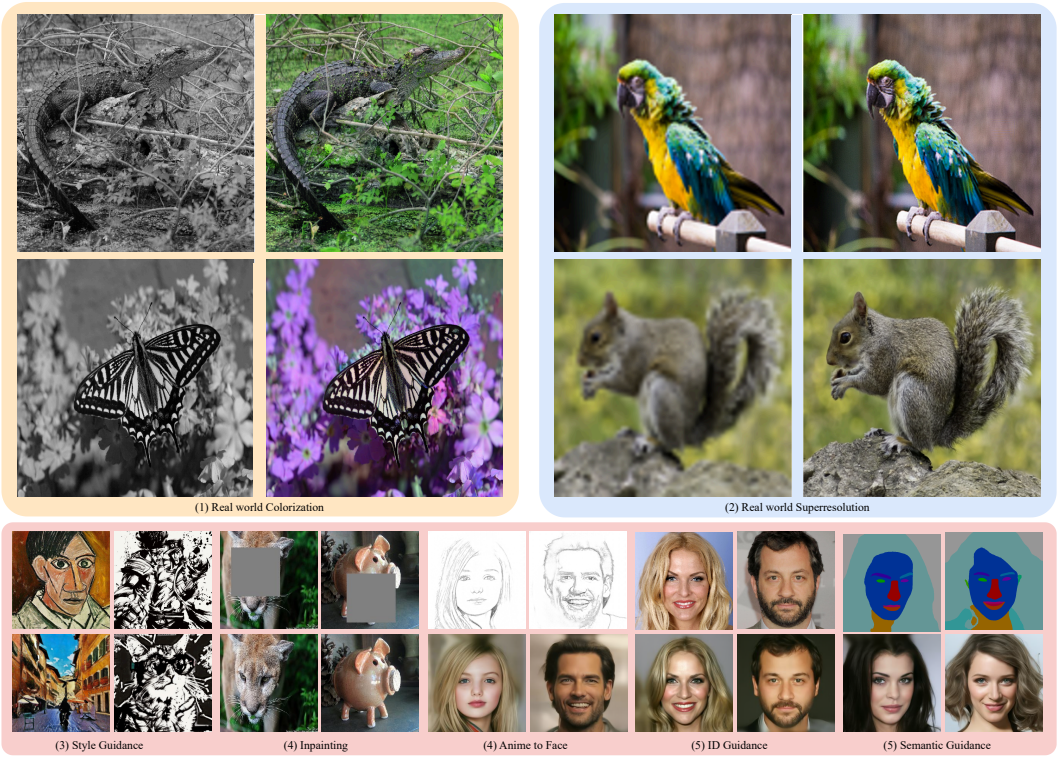

Figure 1: An illustration of the different applications of our method. We utilize a pretrained diffusion model to generate images satisfying a predefined condition without any training, backpropagation through the diffusion U-Net, or any hand-crafted parameter tuning. We present results on (1) real-world colorization, (2) real-world super-resolution, (3) style-guided text-to-image generation, (4) inpainting, (5) sketch-to-face synthesis, (6) face ID guidance, and (7) face semantics–to–face.

training a classifier, which is often undesirable. Some recent works have performed conditional generation without explicit training for the condition by utilizing the implicit guidance capabilities of the diffusion model Chung et al. (2023b); Yu et al. (2023); Nair et al. (2023); Bansal et al. (2023); Chung et al. (2023a). Diffusion Posterior Sampling (DPS) Chung et al. (2023b) proposed using an L_2 loss to solve linear inverse problems with unconditional diffusion models, but often requires many sampling steps for photorealistic results. Freedom Yu et al. (2023) proposed using general loss functions during sampling to achieve training-free conditional sampling. Variants of DPS have also been proposed Song et al. (2023). All the aforementioned loss-guided posterior sampling techniques involve a guidance function at each timestep that requires backpropagation through the diffusion U-Net.

Recently, He et al. (2023) proposed Manifold-Preserving Guided Diffusion Models (MGD) that remove the need for backpropagating through the diffusion U-Net by performing gradient descent with respect to the Minimum Mean-Square Error (MMSE). Although MGD works remarkably well for linear tasks that require more guidance toward the later stages of the sampling process, it may fail in tasks where guidance is needed earlier—for example, face semantics–to–image and sketch–to–image—where stronger guidance is required from much earlier stages. Moreover, like Yu et al. (2023); Nair et al. (2023), MGD also requires a handcrafted parameter on a case-by-case basis. Hence, a generic, lightweight method that works well for both linear and non-linear guidance functions is still missing. The need to find a handcrafted guidance parameter on a case-by-case basis remains an open challenge.

In this paper, we introduce a new framework that can adaptively perform zero-shot generation using diffusion models without manual intervention. We found a simple fix to the problem during the initial timesteps of diffusion: utilize the gradient with respect to the diffusion output noise. Combined with guidance with respect to the MMSE estimate, this combination generalizes well to tasks that require early guidance. Figure 2 visualizes our approach relative to existing works. Using the correction term together with the correction with respect to the MMSE estimate significantly boosts performance in non-linear tasks. We present the corresponding results in Section 6.

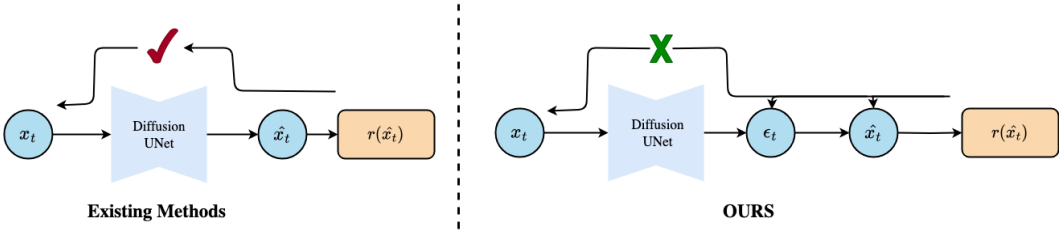

Figure 2: An illustration of the difference between existing methods and ours. Existing works backpropagate through the diffusion network to perform guidance at each timestep, whereas we compute gradients with respect to the MMSE estimate and the predicted noise, thereby bypassing the expensive backpropagation operation.

Moreover, we treat energy-based inference-time guidance Chung et al. (2023b); Yu et al. (2023) as stochastic gradient optimization of the MMSE estimate and the noise present in the image. This formulation enables us to leverage recent research in parameter-free learning Defazio & Mishchenko (2023); Ivgi et al. (2023) to develop a dynamic step-size schedule. This step size adapts to the initial noise seed input of the diffusion model and the guidance functions, thereby removing the need for manual parameter tuning at inference time. Motivated by the effectiveness of differentiable augmentations when training GANs Zhao et al. (2020), we found that utilizing multiple levels of matched differentiable augmentations on the MMSE estimate and the guidance reference significantly improves sampling quality, enabling very high-quality sampling with a low number of guidance steps. We present an overview of the different applications of our method in Figure 1. Specifically, we present results using Stable Diffusion Rombach et al. (2021), unconditional diffusion models released by Nichol & Dhariwal (2021) for 256×256 guidance, and class-conditional diffusion models for high-resolution 512×512 conditional synthesis. The different functionalities of DiffuseGuide are tabulated in Figure 2.

We present experiments on publicly released models on generic images, face images, and Stable Diffusion to show the relevance of our method. We focus on the tasks of (1) inpainting, (2) super-resolution, (3) colorization, (4) Gaussian deblurring, (5) semantic label–to–image generation, (6) face sketch–to–image, and (7) ID guidance and identity generation, and we beat existing benchmarks that utilize diffusion models for these tasks, obtaining a significant performance boost over existing loss-guided methods. To summarize, our contributions are:

2 Related Work

2.1 Training-Free Conditional Sampling Using Diffusion Models

Recently, there has been a rise in works that propose utilizing unconditional diffusion models for conditional sampling Bansal et al. (2023); Chung et al. (2023c); Kawar et al. (2022); Nair et al. (2023). Earlier works proposed solving linear inverse problems using diffusion models with priors dependent on the inverse transform of the degradation. Diffusion Posterior Sampling (DPS) Chung et al. (2023b) considered the degradation to be conditioned on a Gaussian distribution at any intermediate timestep and derived an L_2 regularization at each intermediate timestep to solve linear inverse problems. Freedom Yu et al. (2023) explored an energy-based perspective and extended guidance to non-linear functions using general loss functions. Universal diffusion guidance Aggarwal et al. (2018) extended this guidance process to Stable Diffusion and improved performance using forward–backward guidance. More recent works, such as manifold-guided diffusion He et al. (2023), further constrained the manifold space by projecting the latent space alone. Steered diffusion Nair et al. (2023) guided implicit predictions for non-linear functions, utilizing a hard constraint for normal functions and proposing a plug-and-play module to improve performance.

Table 1: Capabilities of DiffuseGuide versus existing methods for inference-time guidance.

Method	Zeroth order	Linear Tasks	Non-Linear Tasks	Automatic scaling
DPS Chung et al. (2023a)	✗	✓	✗	✗
πGDM Song et al. (2022)	✗	✓	✗	✗
Freedom Yu et al. (2023)	✗	✗	✓	✗
MGD He et al. (2023)	✓	✓	✗	✗
OURS	✓	✓	✓	✓

3 BACKGROUND

3.1 PERTURBED MARKOVIAN KERNEL FOR DIFFUSION TRANSITION

For conditional generation tasks using an unconditional diffusion model, ideally the model would predict intermediates closer to the condition. Let $r(x_t, y)$, where x_t denotes the noisy latent variable at diffusion timestep t and y denotes the conditioning signal (e.g., label or image), give a measure of the distance between an intermediate x_t and the condition y and be a positive, bounded function. Hence, in the reverse process, the diffusion trajectory should proceed through distributions with a higher probability of being closer to the desired cases. We model these trajectory intermediate distributions with

$$\hat{p}(x_t) = p(x_t)r(x_t, y), \tag{1}$$

where $p(x_t)$ is the unconditional marginal distribution of x_t and $\hat{p}(x_t)$ is the perturbed distribution.

Sohl-Dickstein et al. Sohl-Dickstein et al. (2015) first proposed the use of Markovian kernels to estimate the distribution of diffusion intermediates. Specifically, given the state x_t at the equilibrium of the training process for a diffusion model, the distribution at timestep $t-1$ can be estimated as

$$p(x_{t-1}) = \int p(x_t)p_\theta(x_{t-1}|x_t)\, dx_t, \tag{2}$$

where x_{t-1} denotes the latent variable at the next reverse timestep and $p_\theta(x_{t-1}|x_t)$ is the Gaussian transition kernel parameterized by the U-Net θ.

The kernel $p(x_{t-1}|x_t)$ is a Gaussian distribution whose mean can be estimated using the diffusion U-Net and x_t. To estimate a perturbed kernel $\hat{p}(x_{t-1}|x_t)$, the perturbed distribution can be modeled as

$$p(x_{t-1})r(x_{t-1}, y) = \int r(x_t, y)p(x_t)\hat{p}_\theta(x_{t-1}|x_t)\, dx_t. \tag{3}$$

By merging constant terms in the transition into the normalization factor, the transition step can be modeled as

$$\hat{p}_\theta(x_{t-1}|x_t) = p_\theta(x_{t-1}|x_t)\, r(x_{t-1}, y). \tag{4}$$

The proof is given in the Appendix material. Hence, rather than considering a Gaussian posterior, as in DPS Chung et al. (2023b), any distance or loss function can be used. A similar idea was suggested in Steered Diffusion Nair et al. (2023). Another valid transition step of the perturbed process is

$$\hat{p}_\theta(x_{t-1}|x_t) = p_\theta(x_{t-1}|x_t)\frac{r(x_{t-1}, y)}{r(x_t, y)}, \tag{5}$$

which adopts the notion of reciprocal distance from the previous timestep. We establish the relationship between the pertrubed latent distribution and the distance functions, which are revisited in Section 3.3

3.2 INFERENCE-TIME GUIDANCE OF DIFFUSION MODELS

The same formulation can also be viewed in terms of transition probabilities. Consider a pretrained unconditional diffusion model on a specific domain. The problem at hand is to guide the diffusion model during inference time conditioned on y (as defined earlier). Dhariwal et al. Dhariwal & Nichol (2021) proposed a general strategy to perform this by conditioning on y and finding the resultant marginal distribution

$$p(x_{t-1}|x_t, y) = p(x_{t-1}|x_t)\, p(y|x_{t-1}), \tag{6}$$

where x_t is the latent from the previous timestep.

By assuming the distribution $p(y|x_{t-1})$ has much lower curvature compared to $p(x_{t-1}|x_t)$, and considering the marginal distribution close to x_{t-1},

$$\begin{aligned} \log p(y|x_{t-1}) &= (x_{t-1} - \mu)\nabla_{x_{t-1}} \log p(y|x_{t-1}), \\ g &= \nabla_{x_{t-1}} \log p(y|x_{t-1}), \end{aligned} \tag{7}$$

where μ denotes the Gaussian mean in the kernel and g is the conditional gradient.

Plugging back into $\log(p(x_{t-1}|x_t, y))$,

$$\log(p(x_{t-1}|x_t, y)) = (x_{t-1} - \mu - \Sigma g)^T \Sigma^{-1}(x_{t-1} - \mu - \Sigma g) + C, \quad (8)$$
$$p(x_{t-1}|x_t, y) \sim \mathcal{N}(\mu + \Sigma g, \Sigma),$$

where Σ denotes the covariance matrix of the Gaussian kernel and C is a constant.

Hence, the reverse sampling equation becomes

$$x_{t-1} = \frac{1}{\sqrt{\alpha_t}}\left(x_t - \frac{1-\alpha_t}{\sqrt{1-\bar{\alpha}_t}}\epsilon_\theta(x_t)\right) + \sigma_t\epsilon + \Sigma\frac{dr(x_{t-1}, y)}{dx_{t-1}}, \quad \epsilon \sim \mathcal{N}(0, I), \quad (9)$$

where α_t is the noise schedule, $\bar{\alpha}_t = \prod_{i=1}^{t} \alpha_i$ the cumulative variance schedule, $\epsilon_\theta(x_t)$ the noise estimate from the U-Net, and σ_t^2 the variance of the diffusion kernel (so $\Sigma = \sigma_t^2 I$).

3.3 Shortcomings of Existing Methods

Although the energy-based guidance theory supports guidance as a function of the current latent estimate, almost all loss-based guidance techniques derive the distance function as a function of x_t rather than x_{t-1} (both already defined) and compute the gradient based on the previous sample. Although this approach works for many tasks, it requires backpropagating through the neural network and modeling the score function for the guidance correction term. This limits the use of classifier guidance since existing diffusion architectures that produce photorealistic results are often very bulky. One can see why the existing framework that utilizes the derivative with respect to the previous sample works by taking a closer look at Equation (5). As we can see, a reciprocal distance over the previous timestep latent x_t is a valid distance guidance function. In the next section, we elaborate on DiffuseGuide.

4 Proposed Method

As mentioned in the previous section, existing works utilize the derivative with respect to the previous step for guidance; one reason is to use an off-the-shelf auxiliary distance function on the MMSE estimate at each step $\hat{x}_t$, which enables the use of general image-space functions for guidance. Here, the MMSE estimate is defined as

$$\hat{x}_t = \frac{x_t - \sqrt{1-\bar{\alpha}_t}\epsilon_\theta(x_t)}{\sqrt{\bar{\alpha}_t}}, \quad (10)$$

where $\epsilon_\theta(x_t)$ is the noise estimate and $\bar{\alpha}_t$ the cumulative variance schedule.

Another observation is that finding the derivative with respect to the current step requires computing $\hat{x}_{t-1}$, which again requires an additional forward pass through the diffusion network. Hence, the dilemma of backpropagating through the U-Net for guidance remains unresolved.

We found a simple yet effective solution: if we look at the ODE estimate at each step proposed by Song et al. Song et al. (2021a), in the extreme case of deterministic sampling, the next step can be decomposed as

$$x_{t-1} = \sqrt{\alpha_{t-1}}\hat{x}_t + \sqrt{1-\alpha_{t-1}}\epsilon_\theta(x_t). \quad (11)$$

4.1 Double-Descent Classifier Guidance

Rather than perturbing the Gaussian kernel at each timestep, we perturb the components $\hat{x}_t$ and $\epsilon_\theta(x_t)$ by a small amount. Specifically, we perform:

$$\hat{x}_t = \hat{x}_t - c\,\sigma_t^2\frac{\partial r(\hat{x}_t, y)}{\partial \hat{x}_t} \quad (12)$$
$$\epsilon_\theta(x_t) = \epsilon_\theta(x_t) - d\,\sigma_t^2\frac{\partial r(\hat{x}_t, y)}{\partial \epsilon_\theta(x_t)}$$
$$x_{t-1} = \frac{1}{\sqrt{\alpha_t}}\left(x_t - \frac{1-\alpha_t}{\sqrt{1-\bar{\alpha}_t}}\epsilon_\theta(x_t)\right) + \sigma_t\epsilon + c_t\,\sigma_t^2\frac{\partial r(\hat{x}_t, y)}{\partial \hat{x}_t} + d_t\,\sigma_t^2\frac{\partial r(\hat{x}_t, y)}{\partial \epsilon_\theta(x_t)},$$

where c and d are scalar hyperparameters, c_t, d_t are timestep-dependent scaling factors, and σ_t^2 is the diffusion variance at step t.

We perform a *double descent*: descent on $\hat{x_t}$ guides effectively at the end of diffusion where α_{t-1} is close to one, and descent on $\epsilon_\theta(x_t)$ is most effective in early steps. During this descent, we treat the optimization problem like half-quadratic splitting Zhang et al. (2021). Since $\hat{x_t}$ and $\epsilon(x_t)$ are orthogonal at any step, the maximal component of the shift in x_{t-1} due to guidance on $\hat{x_t}$ occurs through $\hat{x_t}$. Hence, we define

$$c_t = -c\sqrt{\alpha_{t-1}}. \tag{13}$$

Similarly, we define d_t as the maximal component of $\epsilon_\theta(x_t)$ in x_{t-1}:

$$d_t = d\,\frac{1-\alpha_t}{\sqrt{\alpha_t}\sqrt{1-\bar{\alpha}_t}}. \tag{14}$$

This provides effective guidance at all timesteps, unlike MGD He et al. (2023), which primarily guides later timesteps. In the following section, we propose an effective empirical estimate for c and d that works for a wide range of tasks.

4.2 A Gradient-Dependent Scaling-Factor Estimate

Distance-over-Gradients (DOG) Ivgi et al. (2023) was proposed as an effective parameter-free dynamic step-size schedule for SGD problems. According to DOG, given any stochastic gradient descent optimization problem, the distance over the gradient works as an effective learning rate. Recent works Wu et al. (2023b) interpret diffusion sampling as a stochastic optimization problem. Inspired by both, we adopt an empirical guidance estimate of the form:

$$\gamma_t = \begin{cases} \frac{1e^{-5}}{\sqrt{\tilde{g}_T^2}}, & \text{if } t = T \\ \frac{\max_{i>t}|f_i - f_T|}{\sqrt{\sum_{i=t}^{T}\tilde{g}_i^2}}, & \text{otherwise,} \end{cases} \tag{15}$$

where $\tilde{g}_t = \nabla_{f_t}\mathcal{L}(f_t, y)$ is the gradient of the chosen loss function with respect to f_t at timestep t, $f_t \in \{\hat{x_t}, x_t, \epsilon_\theta(x_t)\}$, and f_T is the terminal value at the last timestep.

We observed that this empirical estimate works well for first-order sampling involving DPS Chung et al. (2023b) as well. Using Equation (15), we estimate c and d accordingly by substituting f_i as $\hat{x}_t$ and $\epsilon_\theta(x_t)$.

4.3 Differentiable-Augmentation Classifier Guidance

A common practice when performing classifier guidance is to use the noisy estimate at timestep t and compute a loss to regularize the current prediction. However, in many cases, such guidance can produce artifacts and color shifts (see Figure 3 and Figure 5) due to excessive or insufficient guidance at intermediate timesteps that pushes samples off-manifold. An effective solution is to imitate different artifact/color-shift variants on both the source and the target and use these augmented versions to stabilize guidance. We introduce ***DiffuseAugment***, an augmentation strategy for diffusion guidance during inference. Given an intermediate sample x_t and condition y, we augment $\hat{x}_t$ and y with differentiable augmentations:

$$\hat{x}_t^{aug}, y^{aug} = T(\hat{x}_t, y), \tag{16}$$

where $T(\cdot)$ is a differentiable augmentation operator including random cutouts, random translations, and color saturation. The augmentation of y depends on the input signal: for label-based conditioning (e.g., identity or text), we do not augment y; for image-space conditioning, we apply the same random augmentation to y as to x_t. We average the loss across augmentations. We find that DiffuseAugment significantly boosts fidelity and sampling quality. Results are presented in Section 6.

5 Experiments

Because our method applies to both linear and non-linear inverse tasks, for linear tasks we follow DPS and evaluate on two benchmarks: (1) ImageNet Deng et al. (2009) and (2) CelebA Liu et al. (2015).

Method	Inpaint (Box)				Colorization				SR (× 4)				Gaussian Deblur			
	PSNR ↑	SSIM ↑	LPIPS ↓	FID ↓	Cons ↑	SSIM ↑	LPIPS ↓	FID ↓	PSNR ↑	SSIM ↑	LPIPS ↓	FID ↓	PSNR ↑	SSIM ↑	LPIPS ↓	FID ↓
Score-SDE Song et al. (2021b)	9.57	0.329	0.634	94.33	0.1627	0.3996	0.6609	118.86	20.75	0.5844	0.3851	53.22	23.39	0.632	0.361	66.81
ILVR Choi et al. (2021)	-	-	-	-	-	-	-	-	26.14	0.7403	0.2776	52.82	-	-	-	-
DPS Chung et al. (2023a)	19.39	0.610	0.3766	58.89	0.0069	0.5404	0.5594	55.61	17.36	0.4969	0.4613	56.08	20.52	0.5824	0.3756	52.64
MGD He et al. (2023)	27.21	0.7460	0.2197	11.83	0.0018	0.6865	0.4549	38.22	27.51	0.7852	0.2464	60.21	27.23	**0.7695**	0.2327	51.59
Ours	**28.84**	**0.8491**	**0.1432**	**5.96**	**0.0014**	**0.7775**	**0.3036**	**20.89**	**29.47**	**0.8429**	**0.1757**	**46.95**	**27.30**	0.7672	**0.2202**	**42.70**

Table 2: Quantitative evaluation of image restoration tasks on CelebA 256×256-1k with $\sigma_y = 0.05$, We utilize 100 inference steps for all methods

Gaussian Deblurring Colorization Inpainting

Figure 3: Qualitative comparisons for Linear Tasks on CelebA dataset for 100 inference steps

Method	Inpaint (Box)				Colorization				SR (× 4)				Gaussian Deblur			
	PSNR ↑	SSIM ↑	LPIPS ↓	FID ↓	Cons ↑	SSIM ↑	LPIPS ↓	FID ↓	PSNR ↑	SSIM ↑	LPIPS ↓	FID ↓	PSNR ↑	SSIM ↑	LPIPS ↓	FID ↓
Score-SDE Song et al. (2021b)	9.66	0.2087	0.7375	133.54	0.1723	0.3105	0.8197	194.87	14.07	0.2468	0.6766	129.91	15.39	0.3158	0.620	134.67
ILVR Choi et al. (2021)	-	-	-	-	-	-	-	-	15.51	0.4033	0.5253	64.13	-	-	-	-
DPS Chung et al. (2023a)	15.23	0.4261	0.6087	97.90	0.021	0.3774	0.8011	106.25	14.94	0.3258	0.6594	87.26	17.19	0.3980	0.5817	84.74
MGD He et al. (2023)	21.94	0.6920	0.2410	40.30	0.0057	0.5809	0.5427	73.75	23.12	0.6025	0.3936	70.83	23.13	0.6092	0.3695	61.49
Ours	**23.49**	**0.7271**	**0.2001**	**30.72**	**0.0055**	**0.6804**	**0.3362**	**52.76**	**24.23**	**0.6818**	**0.2884**	**43.00**	**23.31**	**0.6157**	**0.3566**	**58.38**

Table 3: Quantitative evaluation of image restoration tasks on ImageNet 256×256-1k with $\sigma_y = 0.05$. **Bold**: best, We utilize 100 inference steps for all methods

For non-linear tasks, we follow Freedom and evaluate using the CelebA dataset. For linear tasks, we evaluate super-resolution (×4), colorization, inpainting (box), and Gaussian deblurring. For non-linear tasks, we evaluate face sketch guidance, face parse-map guidance, and face ID guidance. Since our method is loss-guided, we compare against existing loss-guided sampling methods. Although we acknowledge the parallel line of work on inverse problems without backpropagation Wang et al. (2023); Kawar et al. (2021), we exclude those methods since they tackle only linear inverse problems, whereas loss-guided models are generic.

Implementation Details: We perform all experiments on NVIDIA A6000 GPUs. For ImageNet tasks, we utilize the unconditional model released by Guided Diffusion. For linear face tasks, we use the model trained on the FFHQ dataset Karras et al. (2017) and evaluate on CelebA Liu et al. (2015), as in DPS. For non-linear tasks, we follow Freedom and utilize the unconditional model trained on CelebA. We evaluate using conditions derived from existing networks. For the high-resolution results in Figure 2, we use the class-conditional 512×512 model released by Guided Diffusion. Unless stated otherwise, we use 100 sampling steps. For style transfer, we utilize Stable Diffusion v1.5 Rombach et al. (2021). Our sampling method is generic and compatible with different samplers; in our experiments, we rescaled the DDPM schedule. We fix the number of DiffuseAugment augmentations to 8. For all non-linear tasks, following MGD He et al. (2023), we utilize three time-travel sampling Lugmayr et al. (2022) steps. Even with time-travel sampling, our overall compute time is comparable to Freedom due to savings from bypassing backpropagation through the U-Net (see Appendix). We compare against Freedom (first-order; requires backprop) and MGD. For non-linear tasks, we additionally apply gradient clipping in $(-0.2, 0.2)$. For evaluations, we use MGD, DPS, Score SDE and ILVR. The MGD implementation follows parameters from the original paper (guidance scale 100 for all linear tasks with manifold projection). We detail more on the benchmarks and the guidance functions used in the appendix.

Gaussian Deblurring Colorization Inpainting

Figure 4: Qualitative comparisons for Linear Tasks on ImageNet for 100 inference steps

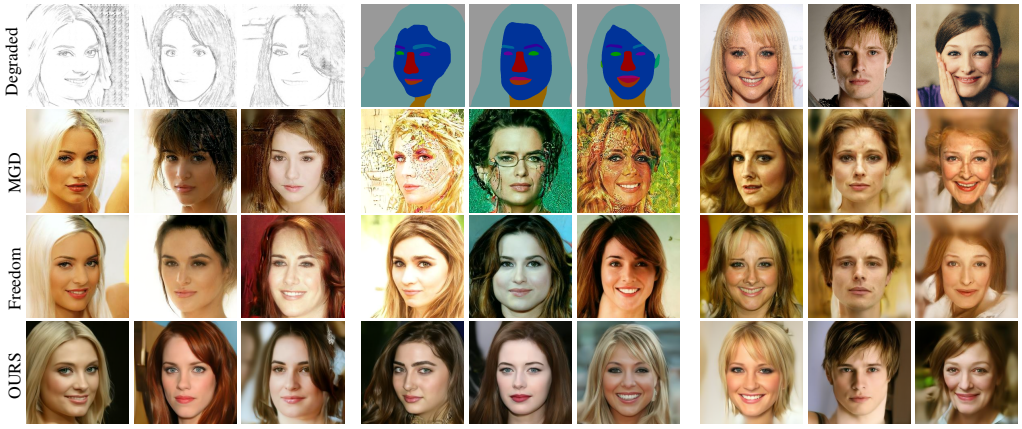

Face-sketch guidance Face-parse guidance ID guidance

Figure 5: Qualitative comparisons for Non-linear Tasks on CelebA dataset for 100 inference steps

Qualitative Analysis: Qualitative face results are given in Figure 3: Gaussian deblurring, super-resolution, and colorization. DPS struggles with 100 diffusion steps because its scaling factor is not strong enough to provide proper guidance within that budget (posterior noise set to 0.05 in all experiments). MGD works well for deblurring and inpainting but fails for colorization, which requires early guidance for natural color flow. In contrast, our method produces more natural images across all cases due to guidance throughout all timesteps. Since restorative face tasks are easier (limited domain), we show ImageNet results in Figure 4. On ImageNet, DPS performance drops more because the problem is more ill-posed (e.g., the eagle example). Our method produces more realistic images, especially in colorization, again due to early gradient flow. For fairness, face models are trained on FFHQ Karras et al. (2017) and tested on CelebA Liu et al. (2015); ImageNet experiments use the validation set. As in Appendix B, we evaluate on CelebA and ImageNet. Results for face restoration are shown in Table 2 and Table 3. SDEdit Meng et al. (2021) fails on face inpainting and colorization because a single perturbation in the noisy domain can push images off-manifold. DPS requires more steps for proper guidance. ILVR is designed for super-resolution; thus we evaluate it only for that task. DPS and MGD apply to all cases. Our approach yields better results than baselines due to guided gradient flow, improving reconstruction quality. On faces, the improvement is most pronounced for colorization (e.g., an 18 FID-point boost over the baseline). ImageNet linear inverse problems are more complex than faces, so overall metrics are lower.

Analysis on Non-Linear Tasks: We compare the performance against Freedom Yu et al. (2023) and MGD He et al. (2023). Figure 5 shows qualitative results. Freedom produces realistic outputs even for the challenging parse-map–to–face task, likely because backpropagating through the U-Net purifies gradient flow. With DiffuseAugment, our gradients are likewise purified, yielding realistic results. MGD does not produce realistic outputs for sketch–to–image and anime–to–face synthesis. We evaluate *Distance* (the L_2 norm between generated and original degradation maps), LPIPS, and FID. Note that artifacts in MGD are not always fully reflected by these metrics. The corresponding

Method	Semantic Parsing			ID Guidance			Face Sketch		
	Distance↓	LPIPS↓	FID↓	Distance↓	LPIPS↓	FID↓	Distance↓	LPIPS↓	FID↓
First-order									
Freedom Yu et al. (2023)	1864.51	0.6030	66.89	0.3767	0.7058	81.40	39.05	0.6583	86.51
Zeroth-order									
MGD He et al. (2023)	**2698.27**	0.6995	104.32	0.4291	0.7178	92.61	39.34	0.6576	70.42
Ours	2722.51	**0.6199**	**79.42**	**0.3780**	**0.5932**	**82.70**	**39.03**	**0.5509**	**69.51**

Table 4: Non-linear tasks. Best results out of zeroth-order optimization algorithms are highlighted.

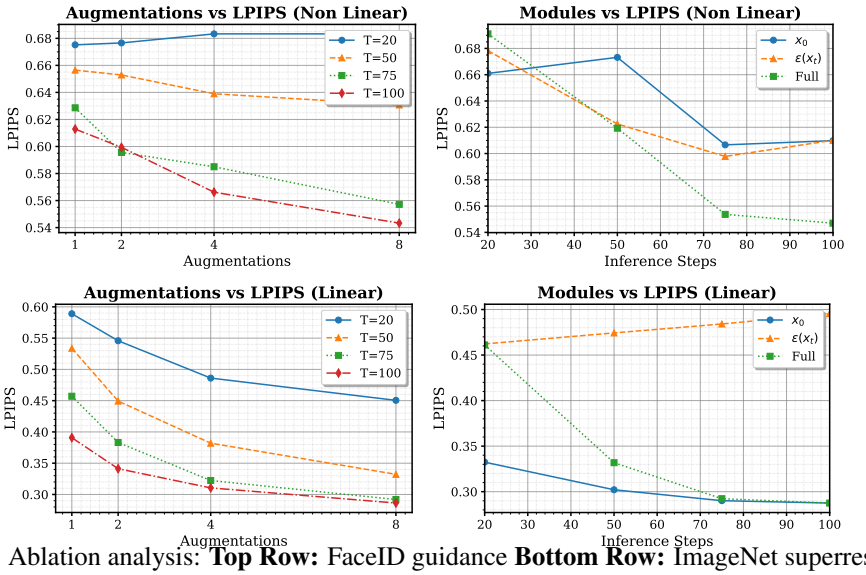

Figure 6: Ablation analysis: **Top Row:** FaceID guidance **Bottom Row:** ImageNet superresolution

metrics are in Section 5. Compared to first-order methods, we obtain better FID and LPIPS across all cases, with significantly lower compute than Freedom.

6 Ablation Studies

We perform extensive ablations on the effect of DiffuseAugment and on each guidance term. For ablations, we use 100 images and report average LPIPS due to the volume of experiments.

Effect of DiffuseAugment: We vary the number of augmentations for both linear and non-linear tasks. For the linear task, we choose ImageNet super-resolution ($\times 4$). We vary diffusion steps $T \in \{20, 50, 75, 100\}$ and report average LPIPS. For linear tasks, even with low T (e.g., $T = 20$), increasing augmentations to 8 markedly improves perceptual quality, matching $T = 50$ with only two augmentations. For non-linear tasks, the benefit is muted or negative at $T = 20$ because most $\hat{x}_t$ remain too noisy for the guidance network (e.g., ArcFace Deng et al. (2019)), which yields irregular gradients. As T increases and gradients stabilize, DiffuseAugment yields substantial gains.

Effect of Different Guidance Components: Figure 6 ablates different terms (DiffuseAugment fixed at 1; time-travel sampling off). Guiding with $\hat{x}_t$ alone shows a performance dip for small T; early guidance through $\hat{x}_t$ is weak, and time-travel sampling (if used) would require careful tuning. Guiding via the output noise ϵ_t helps when T is small, but the effect diminishes as T increases. Our double-descent guidance provides both early and late guidance, improving perceptual quality—especially for non-linear inverse problems where gradient estimates are noisier. For linear inverse problems, double descent offers smaller gains and can slightly degrade performance in some settings (see Figure 6). Additional examples are in the Appendix.

7 Conclusion

We proposed an improvement to loss-guided, zero-shot conditional generation with unconditional diffusion models. Specifically, we introduced a sampling technique that removes the need to back-propagate through the diffusion U-Net, enabling guidance for general inverse problems. We also proposed an empirical, automatic scaling function that removes manual tuning of guidance scales and start/end guidance steps. Finally, we introduced a differentiable data-augmentation method that significantly improves sampling fidelity. We demonstrated results across four linear and three non-linear tasks on faces and natural images. Our sampling technique produces photorealistic samples with lower sampling time and higher fidelity than existing methods.

8 ETHICS STATEMENT

This work studies generative modeling from a theoretical and methodological perspective. All datasets used (ImageNet,CelebA, FFHQ) are publicly available and widely adopted in research, involving no human subjects or private data. While generative models may be misused to create harmful content, our contributions are intended solely to advance scientific understanding and efficiency of visual generation. We declare no conflicts of interest, and all results are reproducible with the code and checkpoints that will be released.

9 REPRODUCIBILITY STATEMENT

We have taken steps to ensure reproducibility of our results. The datasets are publicly available and described in the appendix. Model architecture, training details, and hyperparameters are provided in Section 4 and Appendix. We report all experimental protocols, ablations, and evaluation metrics. Code, pretrained checkpoints, and instructions to reproduce our results will be released upon publication.

REFERENCES

Hemant K Aggarwal, Merry P Mani, and Mathews Jacob. MoDL: Model-based deep learning architecture for inverse problems. *IEEE transactions on medical imaging*, 38(2):394–405, 2018.

Martin Arjovsky, Soumith Chintala, and Léon Bottou. Wasserstein generative adversarial networks. In *International conference on machine learning*, pp. 214–223. PMLR, 2017.

Yogesh Balaji, Seungjun Nah, Xun Huang, Arash Vahdat, Jiaming Song, Karsten Kreis, Miika Aittala, Timo Aila, Samuli Laine, Bryan Catanzaro, et al. ediffi: Text-to-image diffusion models with an ensemble of expert denoisers. *arXiv preprint arXiv:2211.01324*, 2022.

Arpit Bansal, Hong-Min Chu, Avi Schwarzschild, Soumyadip Sengupta, Micah Goldblum, Jonas Geiping, and Tom Goldstein. Universal guidance for diffusion models. *arXiv preprint arXiv:2302.07121*, 2023.

Andreas Blattmann, Robin Rombach, Huan Ling, Tim Dockhorn, Seung Wook Kim, Sanja Fidler, and Karsten Kreis. Align your latents: High-resolution video synthesis with latent diffusion models. In *Proceedings of the IEEE/CVF Conference on Computer Vision and Pattern Recognition*, pp. 22563–22575, 2023.

Stanley H Chan, Xiran Wang, and Omar A Elgendy. Plug-and-play admm for image restoration: Fixed-point convergence and applications. *IEEE Transactions on Computational Imaging*, 3(1): 84–98, 2016.

Jooyoung Choi, Sungwon Kim, Yonghyun Jeong, Youngjune Gwon, and Sungroh Yoon. Ilvr: Conditioning method for denoising diffusion probabilistic models. *arXiv preprint arXiv:2108.02938*, 2021.

Hyungjin Chung, Jeongsol Kim, Michael Thompson Mccann, Marc Louis Klasky, and Jong Chul Ye. Diffusion posterior sampling for general noisy inverse problems. In *International Conference on Learning Representations*, 2023a. URL https://openreview.net/forum?id=OnD9zGAGT0k.

Hyungjin Chung, Dohoon Ryu, Michael T Mccann, Marc L Klasky, and Jong Chul Ye. Solving 3d inverse problems using pre-trained 2d diffusion models. *IEEE/CVF Conference on Computer Vision and Pattern Recognition*, 2023b.

Hyungjin Chung, Jong Chul Ye, Peyman Milanfar, and Mauricio Delbracio. Prompt-tuning latent diffusion models for inverse problems. *ArXiv*, abs/2310.01110, 2023c.

Aaron Defazio and Konstantin Mishchenko. Learning-rate-free learning by d-adaptation. *arXiv preprint arXiv:2301.07733*, 2023.

Jia Deng, Wei Dong, Richard Socher, Li-Jia Li, Kai Li, and Li Fei-Fei. Imagenet: A large-scale hierarchical image database. In *2009 IEEE conference on computer vision and pattern recognition*, pp. 248–255. Ieee, 2009.

Jiankang Deng, Jia Guo, Niannan Xue, and Stefanos Zafeiriou. Arcface: Additive angular margin loss for deep face recognition. In *Proceedings of the IEEE/CVF conference on computer vision and pattern recognition*, pp. 4690–4699, 2019.

Prafulla Dhariwal and Alexander Nichol. Diffusion models beat gans on image synthesis. *Advances in Neural Information Processing Systems*, 34, 2021.

Ian Goodfellow, Jean Pouget-Abadie, Mehdi Mirza, Bing Xu, David Warde-Farley, Sherjil Ozair, Aaron Courville, and Yoshua Bengio. Generative adversarial networks. *Communications of the ACM*, 63(11):139–144, 2020.

Alexandros Graikos, Nikolay Malkin, Nebojsa Jojic, and Dimitris Samaras. Diffusion models as plug-and-play priors. *arXiv preprint arXiv:2206.09012*, 2022.

Yutong He, Naoki Murata, Chieh-Hsin Lai, Yuhta Takida, Toshimitsu Uesaka, Dongjun Kim, Wei-Hsiang Liao, Yuki Mitsufuji, J Zico Kolter, Ruslan Salakhutdinov, et al. Manifold preserving guided diffusion. *arXiv preprint arXiv:2311.16424*, 2023.

Jonathan Ho, Ajay Jain, and Pieter Abbeel. Denoising diffusion probabilistic models. *Advances in Neural Information Processing Systems*, 33:6840–6851, 2020.

Jonathan Ho, William Chan, Chitwan Saharia, Jay Whang, Ruiqi Gao, Alexey Gritsenko, Diederik P Kingma, Ben Poole, Mohammad Norouzi, David J Fleet, et al. Imagen video: High definition video generation with diffusion models. *arXiv preprint arXiv:2210.02303*, 2022.

MD Zakir Hossain, Ferdous Sohel, Mohd Fairuz Shiratuddin, and Hamid Laga. A comprehensive survey of deep learning for image captioning. *ACM Computing Surveys (CsUR)*, 51(6):1–36, 2019.

Maor Ivgi, Oliver Hinder, and Yair Carmon. Dog is sgd's best friend: A parameter-free dynamic step size schedule. *arXiv preprint arXiv:2302.12022*, 2023.

Heewoo Jun and Alex Nichol. Shap-e: Generating conditional 3d implicit functions. *arXiv preprint arXiv:2305.02463*, 2023.

Tero Karras, Timo Aila, Samuli Laine, and Jaakko Lehtinen. Progressive growing of GANs for improved quality, stability, and variation. *arXiv preprint arXiv:1710.10196*, 2017.

Bahjat Kawar, Gregory Vaksman, and Michael Elad. Stochastic image denoising by sampling from the posterior distribution. In *Proceedings of the IEEE/CVF International Conference on Computer Vision (ICCV) Workshops*, pp. 1866–1875, October 2021.

Bahjat Kawar, Michael Elad, Stefano Ermon, and Jiaming Song. Denoising diffusion restoration models. *arXiv preprint arXiv:2201.11793*, 2022.

Ziwei Liu, Ping Luo, Xiaogang Wang, and Xiaoou Tang. Deep learning face attributes in the wild. In *Proceedings of International Conference on Computer Vision (ICCV)*, December 2015.

Andreas Lugmayr, Martin Danelljan, Andres Romero, Fisher Yu, Radu Timofte, and Luc Van Gool. Repaint: Inpainting using denoising diffusion probabilistic models. In *Proceedings of the IEEE/CVF Conference on Computer Vision and Pattern Recognition*, pp. 11461–11471, 2022.

Chenlin Meng, Yang Song, Jiaming Song, Jiajun Wu, Jun-Yan Zhu, and Stefano Ermon. SDEdit: Image synthesis and editing with stochastic differential equations. *arXiv preprint arXiv:2108.01073*, 2021.

Nithin Gopalakrishnan Nair, Anoop Cherian, Suhas Lohit, Ye Wang, Toshiaki Koike-Akino, Vishal M Patel, and Tim K Marks. Steered diffusion: A generalized framework for plug-and-play conditional image synthesis. In *Proceedings of the IEEE/CVF International Conference on Computer Vision*, pp. 20850–20860, 2023.

Anh Nguyen, Jeff Clune, Yoshua Bengio, Alexey Dosovitskiy, and Jason Yosinski. Plug & play generative networks: Conditional iterative generation of images in latent space. In *Proceedings of the IEEE conference on computer vision and pattern recognition*, pp. 4467–4477, 2017.

Alexander Quinn Nichol and Prafulla Dhariwal. Improved denoising diffusion probabilistic models. In *International Conference on Machine Learning*, pp. 8162–8171. PMLR, 2021.

Ben Poole, Ajay Jain, Jonathan T. Barron, and Ben Mildenhall. Dreamfusion: Text-to-3d using 2d diffusion. *arXiv*, 2022.

Alec Radford, Luke Metz, and Soumith Chintala. Unsupervised representation learning with deep convolutional generative adversarial networks. *arXiv preprint arXiv:1511.06434*, 2015.

Robin Rombach, Andreas Blattmann, Dominik Lorenz, Patrick Esser, and Björn Ommer. High-resolution image synthesis with latent diffusion models, 2021.

Chitwan Saharia, William Chan, Huiwen Chang, Chris Lee, Jonathan Ho, Tim Salimans, David Fleet, and Mohammad Norouzi. Palette: Image-to-image diffusion models. In *ACM SIGGRAPH 2022 Conference Proceedings*, pp. 1–10, 2022a.

Chitwan Saharia, Jonathan Ho, William Chan, Tim Salimans, David J Fleet, and Mohammad Norouzi. Image super-resolution via iterative refinement. *IEEE Transactions on Pattern Analysis and Machine Intelligence*, 2022b.

Maximilian Seitzer. pytorch-fid: FID Score for PyTorch. `https://github.com/mseitzer/pytorch-fid`, August 2020. Version 0.3.0.

Karen Simonyan and Andrew Zisserman. Very deep convolutional networks for large-scale image recognition. *arXiv preprint arXiv:1409.1556*, 2014.

Jascha Sohl-Dickstein, Eric Weiss, Niru Maheswaranathan, and Surya Ganguli. Deep unsupervised learning using nonequilibrium thermodynamics. In *International Conference on Machine Learning*, pp. 2256–2265. PMLR, 2015.

Jiaming Song, Chenlin Meng, and Stefano Ermon. Denoising diffusion implicit models. In *9th International Conference on Learning Representations, ICLR*, 2021a.

Jiaming Song, Arash Vahdat, Morteza Mardani, and Jan Kautz. Pseudoinverse-guided diffusion models for inverse problems. In *International Conference on Learning Representations*, 2022.

Jiaming Song, Qinsheng Zhang, Hongxu Yin, Morteza Mardani, Ming-Yu Liu, Jan Kautz, Yongxin Chen, and Arash Vahdat. Loss-guided diffusion models for plug-and-play controllable generation. In *International Conference on Machine Learning*, pp. 32483–32498. PMLR, 2023.

Yang Song, Jascha Sohl-Dickstein, Diederik P Kingma, Abhishek Kumar, Stefano Ermon, and Ben Poole. Score-based generative modeling through stochastic differential equations. In *International Conference on Learning Representations*, 2021b. URL `https://openreview.net/forum?id=PxTIG12RRHS`.

Ting-Chun Wang, Ming-Yu Liu, Jun-Yan Zhu, Andrew Tao, Jan Kautz, and Bryan Catanzaro. High-resolution image synthesis and semantic manipulation with conditional gans. In *Proceedings of the IEEE conference on computer vision and pattern recognition*, pp. 8798–8807, 2018.

Yinhuai Wang, Jiwen Yu, and Jian Zhang. Zero-shot image restoration using denoising diffusion null-space model. In *The Eleventh International Conference on Learning Representations*, 2023. URL `https://openreview.net/forum?id=mRieQgMtNTQ`.

Jay Zhangjie Wu, Yixiao Ge, Xintao Wang, Stan Weixian Lei, Yuchao Gu, Yufei Shi, Wynne Hsu, Ying Shan, Xiaohu Qie, and Mike Zheng Shou. Tune-a-video: One-shot tuning of image diffusion models for text-to-video generation. In *Proceedings of the IEEE/CVF International Conference on Computer Vision*, pp. 7623–7633, 2023a.

Zike Wu, Pan Zhou, Kenji Kawaguchi, and Hanwang Zhang. Fast diffusion model. *arXiv preprint arXiv:2306.06991*, 2023b.

Xiaoyu Xiang, Ding Liu, Xiao Yang, Yiheng Zhu, Xiaohui Shen, and Jan P Allebach. Adversarial open domain adaptation for sketch-to-photo synthesis. In *Proceedings of the IEEE/CVF Winter Conference on Applications of Computer Vision*, pp. 1434–1444, 2022.

Changqian Yu, Jingbo Wang, Chao Peng, Changxin Gao, Gang Yu, and Nong Sang. Bisenet: Bilateral segmentation network for real-time semantic segmentation. In *Proceedings of the European conference on computer vision (ECCV)*, pp. 325–341, 2018.

Jiwen Yu, Yinhuai Wang, Chen Zhao, Bernard Ghanem, and Jian Zhang. Freedom: Training-free energy-guided conditional diffusion model. *arXiv preprint arXiv:2303.09833*, 2023.

Kai Zhang, Yawei Li, Wangmeng Zuo, Lei Zhang, Luc Van Gool, and Radu Timofte. Plug-and-play image restoration with deep denoiser prior. *IEEE Transactions on Pattern Analysis and Machine Intelligence*, 44(10):6360–6376, 2021.

Richard Zhang, Phillip Isola, Alexei A Efros, Eli Shechtman, and Oliver Wang. The unreasonable effectiveness of deep features as a perceptual metric. In *CVPR*, 2018.

Shengyu Zhao, Zhijian Liu, Ji Lin, Jun-Yan Zhu, and Song Han. Differentiable augmentation for data-efficient gan training. *Advances in neural information processing systems*, 33:7559–7570, 2020.

APPENDIX

A EVALUATION BENCHMARK DETAILS:

We evaluate four tasks. For inpainting, we choose a random box mask of size 128×128 pixels. For Gaussian deblurring, we apply a 61×61 Gaussian blur with kernel intensity 3.0. For super-resolution, we downsample images using bicubic downsampling to 64×64. We report PSNR and SSIM for restoration quality, LPIPS Zhang et al. (2018) for perceptual similarity, and FID Seitzer (2020) for distributional similarity. For colorization, we also report a consistency measure: the MSE between grayscale versions of the reconstruction and the original image (lower is better). For non-linear inverse functions, we evaluate three tasks: face parse guidance, face ID guidance, and face sketch guidance. For sketches, we utilize an open-source pretrained network that converts faces to sketches Xiang et al. (2022). We also evaluate Score-SDE Meng et al. (2021). For super-resolution we additionally evaluate the zero-shot method ILVR Choi et al. (2021).

B GUIDANCE FUNCTIONS UTILIZED:

For colorization, we convert to YCbCr and take the Y component as the measurement. We compare two loss-guided diffusion methods: DPS Chung et al. (2023b) and MGD He et al. (2023). We use 1000 images from CelebA Liu et al. (2015) as in Freedom Yu et al. (2023) and obtain the corresponding non-linear map for each image . As the guidance function for sketches, we use the Euclidean distance between the generated sketch from $\hat{x}_t$ and the target sketch. For face parse guidance, we utilize BiSeNet Yu et al. (2018) to derive parse maps from $\hat{x}_t$ and use the Euclidean distance between predicted and ground-truth labels. For face ID guidance, we use Deng et al. (2019) to obtain face embeddings and measure cosine-similarity loss.

C ALGORITHM OF DIFFUSEGUIDER

We present the over algorithm of dreamguider without time travel sampling and the parameter estimation algorithm in Algorithm 1

D PROOF FOR PERTURBED MARKOVIAN KERNEL EQUATION

In the main paper, we emphasized that any positive distance function can be utilized for performing conditional generation using the perturbed Markovian kernel equation. hHre we proceed to derive the perturbed transition step. For the proof we closely follow the work from Dickenson et al Sohl-Dickstein et al. (2015). Given a unconditional transition distribution $p_\theta(x_{t-1}|x_t)$ and a distance function $r(., y)$, where y is the condition provided Please note that we assume $r(., y)$ has relatively small variance compared to $p_\theta(x_{t-1}|x_t)$, We know that at equilibrium state, the distribution at any timestep t ina diffusion model can be written as

$$p(x_{t-1}) = \int p(x_t) p_\theta(x_{t-1}|x_t) dx_t. \tag{17}$$

To estimate a perturbed transition kernel $\hat{p}(x_{t-1}|x_t)$,we start the perturbed distribution as

$$p(x_{t-1}) r(x_{t-1}, y) = \int r(x_t, y) p(x_t) \hat{p}_\theta(x_{t-1}|x_t) dx_t. \tag{18}$$

By simple algebraic manipulations, taking $r(x_{t-1}, y)$ to the other side, we get

$$p(x_{t-1}) = \int \frac{r(x_t, y)}{r(x_{t-1}, y)} p(x_t) \hat{p}_\theta(x_{t-1}|x_t) dx_t. \tag{19}$$

Algorithm 1 Dreamguider

Input: distance function $r(, .y)$, condition y , Timesteps T

$x_T \sim \mathcal{N}(x_T; 0, I)$
for $t = T - 1, \ldots, 1$ **do**
  $\Sigma = \sqrt{1 - \bar{\alpha}_t}$
  $\epsilon \sim \mathcal{N}(\epsilon; 0, I)$
  $\hat{x}_t = \frac{x_t - \sqrt{1-\bar{\alpha}_t}\epsilon_\theta(x_t)}{\sqrt{\bar{\alpha}_t}}$
  Compute $\frac{dr(\hat{x}_t, y)}{d\hat{x}_t}$, $\frac{dr(\hat{x}_t, y)}{d\epsilon_\theta(x_t)}$
  update $c = ESTIMATE(t, \epsilon_\theta(x_t), \frac{dr(\hat{x}_t, y)}{d\epsilon_\theta(x_t)})$
  update $d = ESTIMATE(t, \hat{x}_t, \frac{dr(\hat{x}_t, y)}{d\hat{x}_t})$
  $c_t = c\sqrt{\alpha_{t-1}}$
  $d_t = -d.\frac{1-\alpha_t}{\sqrt{\alpha_t}\sqrt{1-\bar{\alpha}_t}}$
  $x_{t-1} = \frac{1}{\sqrt{\alpha_t}}\left(x_t - \frac{1-\alpha_t}{\sqrt{1-\bar{\alpha}_t}}\epsilon_\theta(x_t)\right) + \sigma_t\epsilon - c_t\Sigma\frac{dr(\hat{x}_t, y)}{d\hat{x}_t} - d_t\Sigma\frac{dr(\hat{x}_t, y)}{d\epsilon_\theta(x_t)}$
end for
function ESTIMATE(t, f_i, g_t)
  if $t = T$ **then**
    $\gamma_t = \frac{1e^{-5}}{\sqrt{g_T^2}}$
    Store f_T,
  else
    $\gamma_t = \frac{\max i>t|f_i - f_T|}{\sqrt{\Sigma_{i=i}^T g_t^2}}$
  end if
  Store $\sqrt{\Sigma_{i=i}^T g_t^2}$
  return γ_t
end function return x_0

By comparing Equation (17) and Equation (19) we can see that one solution for the transitional distribution is

$$\hat{p}_\theta(x_{t-1}|x_t) = p_\theta(x_{t-1}|x_t)\frac{r(x_{t-1}, y)}{r(x_t, y)}. \tag{20}$$

Also since normalization constants doesn't affect the score function or transition step, Absorbing x_t to the normalization factor of $p_\theta(x_{t-1}|x_t)$, another valid perturbed transition kernel is

$$\hat{p}_\theta(x_{t-1}|x_t) = p_\theta(x_{t-1}|x_t)\frac{r(x_{t-1}, y)}{Z}. \tag{21}$$

Please note that the term Z does not affect the transition step in the reverse process when the variance of $r(., y)$ is small.

Method	Freedom	Dreamguider(1)	Dreamguider(2)	Dreamguider(3)
Sketch to Face	24.95	17.55	27.04	35.09
FaceID to Face	24.94	20.45	31.89	41.80
FaceParse to Face	56.25	48.35	75.43	107.02

Table 5: Non-linear tasks ablation analysis on time taken, the value is represented in seconds

E Time comparison for Dreamguider with timetravel sampling and Freedom(First order) for non linear tasks

We present the time taken by Freedom, a first order algorithm for one step of time travel sampling Lugmayr et al. (2022); Yu et al. (2023) in Table 5

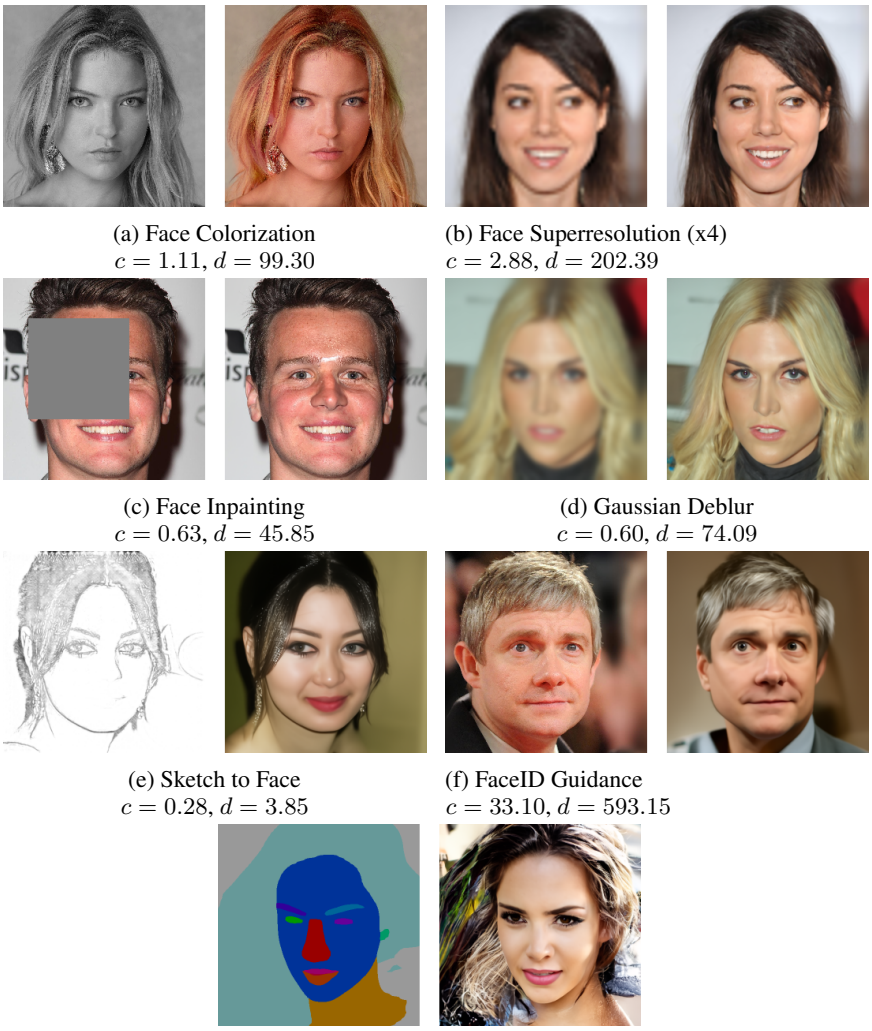

(a) Face Colorization
$c = 1.11$, $d = 99.30$

(b) Face Superresolution (x4)
$c = 2.88$, $d = 202.39$

(c) Face Inpainting
$c = 0.63$, $d = 45.85$

(d) Gaussian Deblur
$c = 0.60$, $d = 74.09$

(e) Sketch to Face
$c = 0.28$, $d = 3.85$

(f) FaceID Guidance
$c = 33.10$, $d = 593.15$

(g) Parsemaps to Face
$c = 0.001$, $d = 0.13$

Figure 7: Figure illustrating the guidance scales for different tasks.

F Estimated parameter value for different tasks

In this section, we present the result and the parameter estimated by our approach for different tasks. For this experiment, we use 100 timesteps of diffusion and present the value at the 100th timestep. Here we define d as the scaling factor of the scaling constant of the the loss derivative relative to $\epsilon_\theta(x_t)$ and c as that of $\hat{x}_t$ as in the main paper . The corresponding results are shown in Figure 7

G Future Work

Although we illustrated the approach across various tasks for pixel-space diffusion models, the direct approach cannot be used for latent diffusion models on linear inverse problems without additional time-travel sampling steps, which increases compute due to VAE reconstruction error. In future work, we will explore optimization strategies to mitigate this. Moreover, while the empirical DOG-based estimate works well across tasks and suggests the existence of an optimal parameter, a thorough mathematical analysis to obtain truly optimal parameters remains open.

H LLM USAGE

We acknowledge that Large Language Models (LLMs) were used to assist with refining the clarity of the writing in this manuscript.

I NON CHERRY PICKED RESULTS FOR DIFFERENT TASKS.

Figure 8: Figure illustrating **Non cherry picked** results for ImageNet colorization

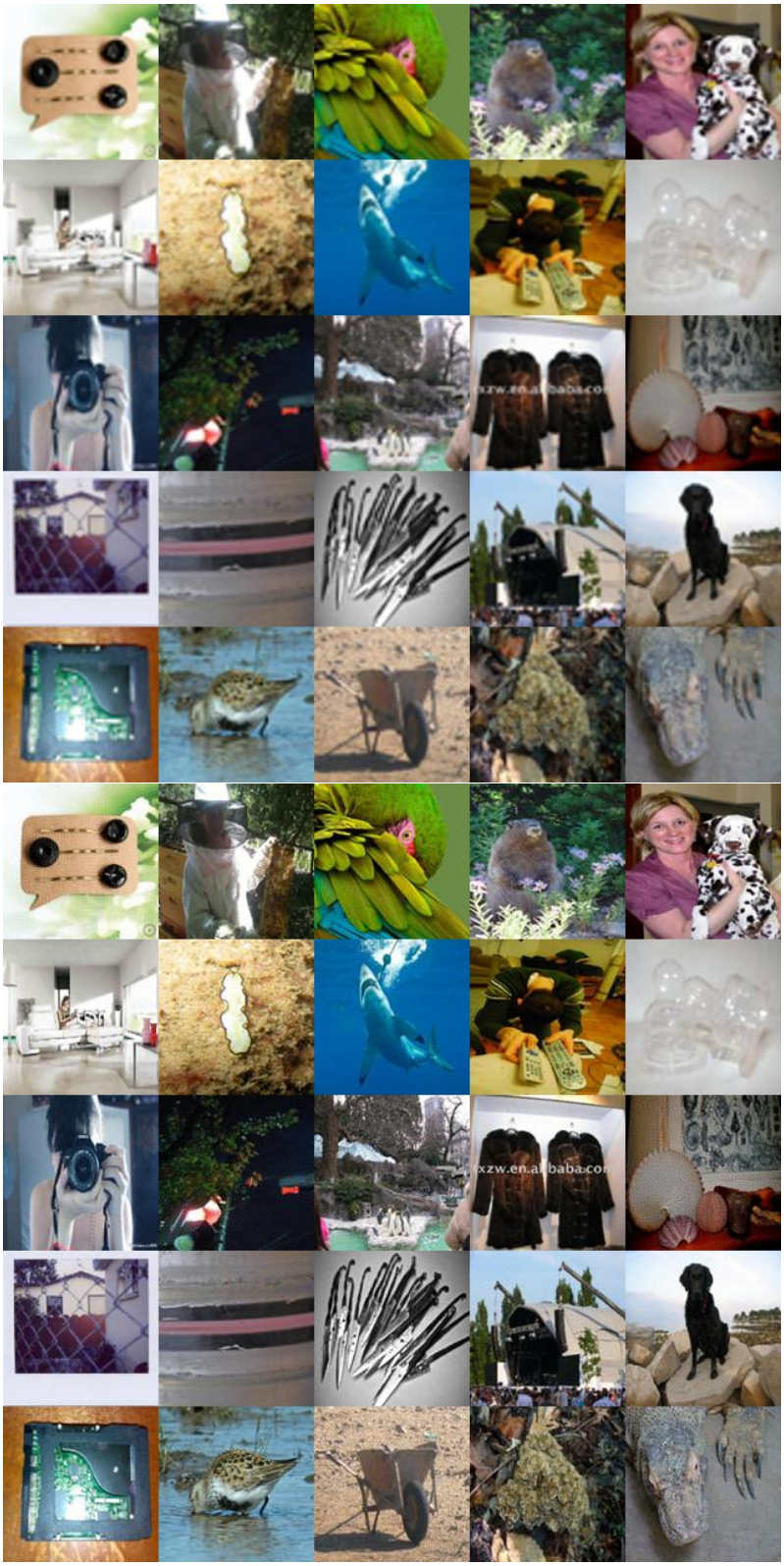

Figure 9: Figure illustrating **Non cherry picked** results for ImageNet superresolution

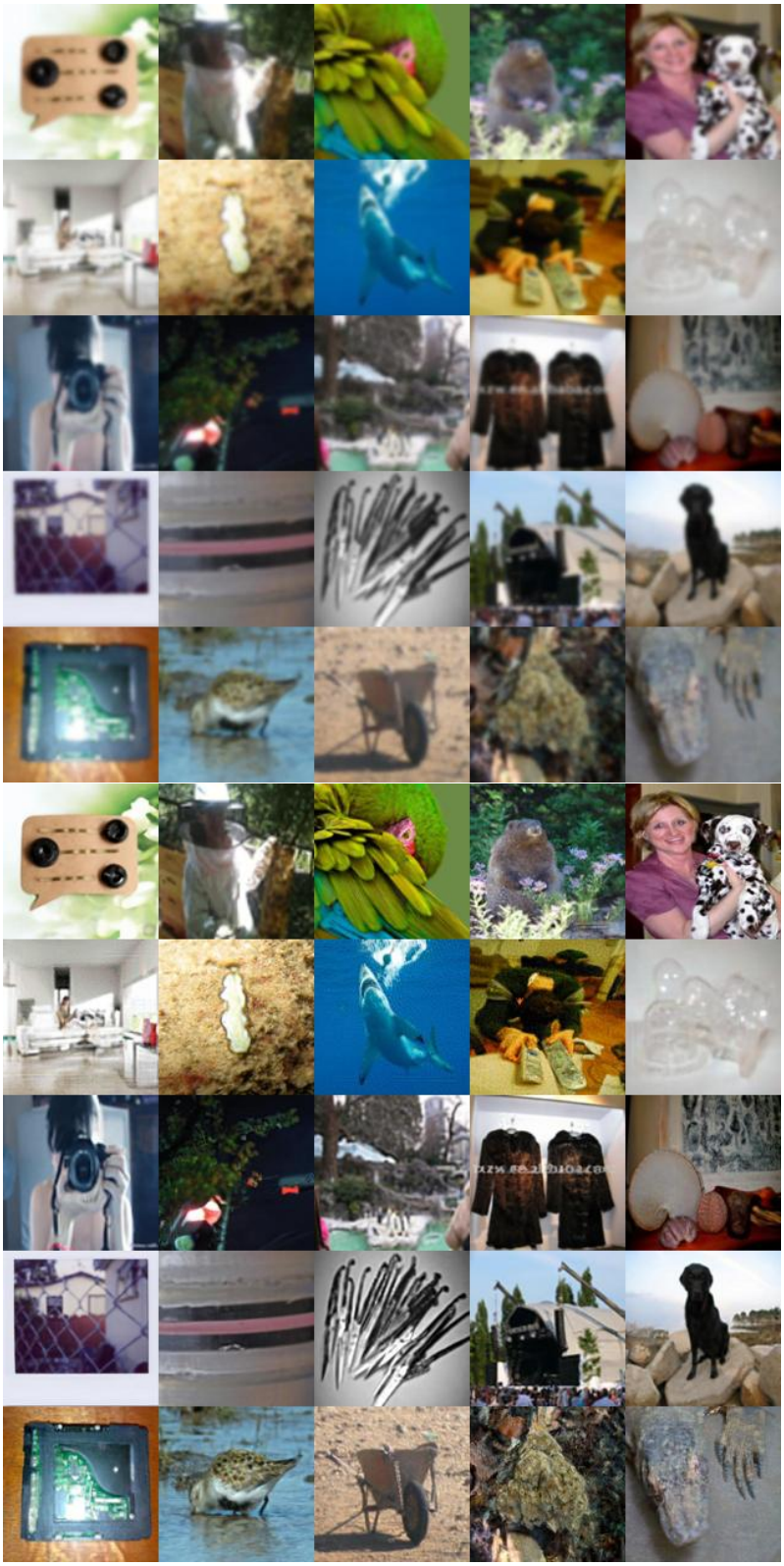

Figure 10: Figure illustrating **Non cherry picked** results for Gaussian deblurring on ImageNet

Figure 11: Figure illustrating **Non cherry picked** results for face colorization

Figure 12: Figure illustrating **Non cherry picked** results for face superresolution

Figure 13: Figure illustrating **Non cherry picked** results for Gaussian Deblurring

Figure 14: Figure illustrating **Non cherry picked** results for face inpainting

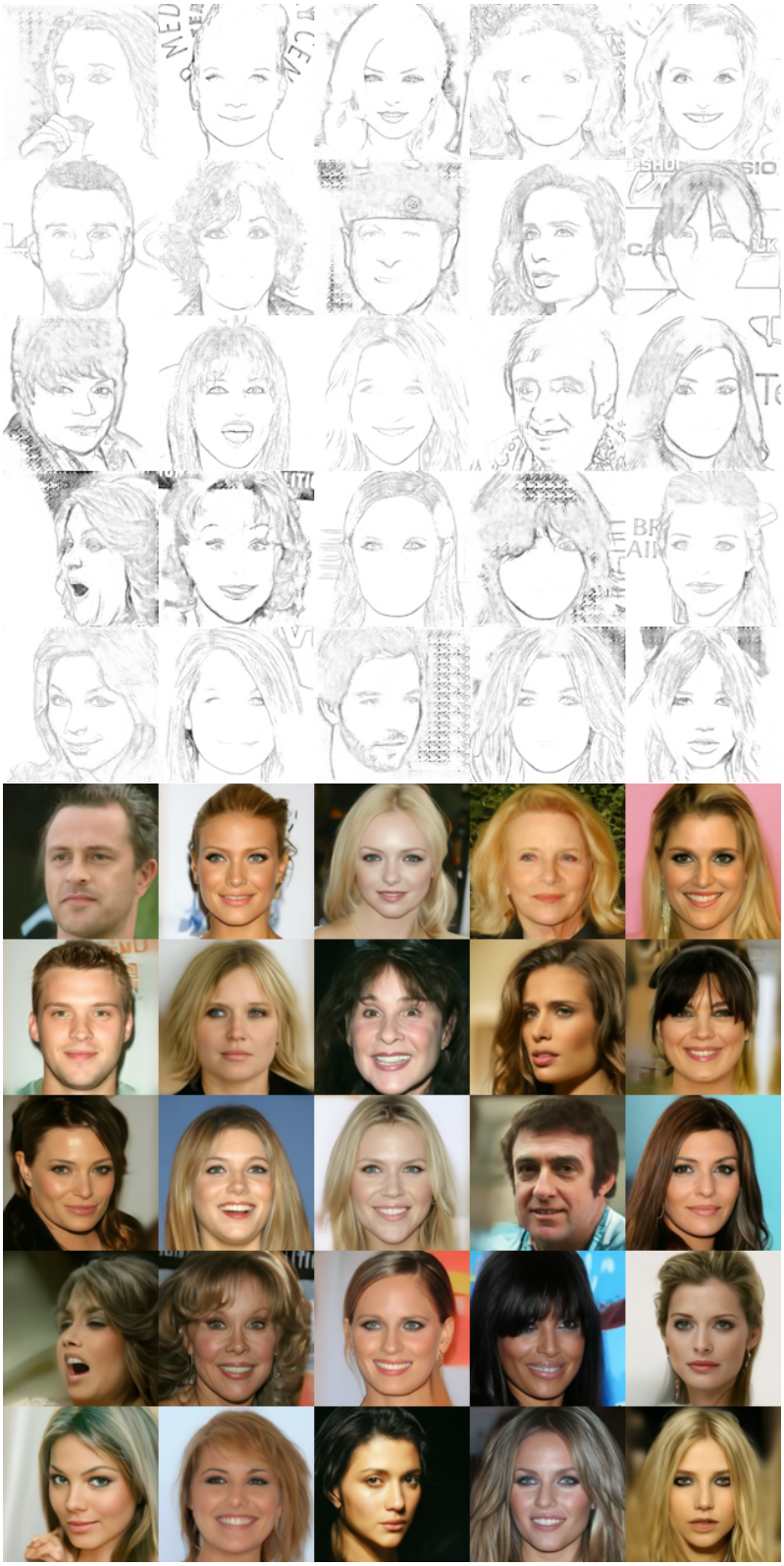

Figure 15: Figure illustrating **Non cherry picked** results for sketch to face synthesis

Figure 16: Figure illustrating **Non cherry picked** results for Face ID guidance

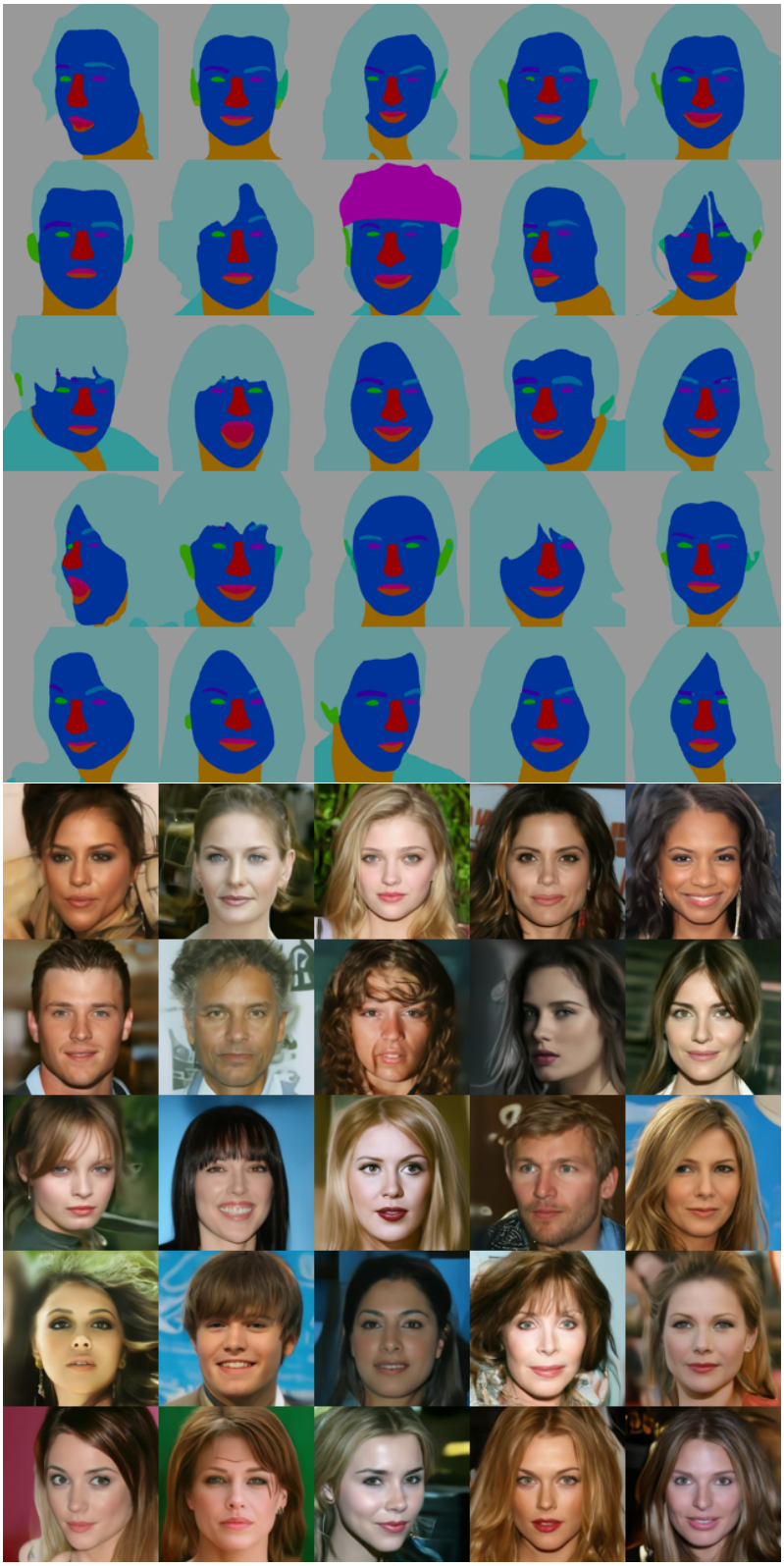

Figure 17: Figure illustrating **Non cherry picked** results for Face Parse Guidance